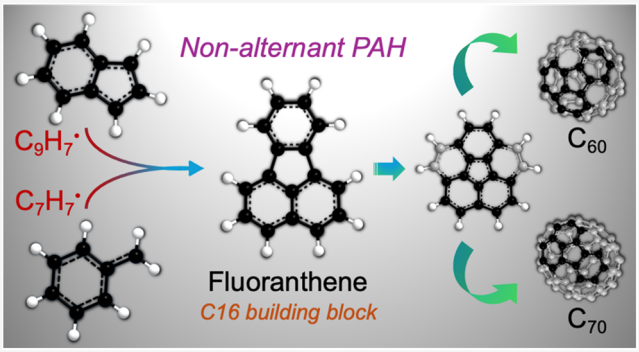
JACS
JOURNAL OF THE AMERICAN CHEMICAL SOCIETY
pubs.acs.org/JACS
Article

Indenyl-Benzyl Radical Recombination Leads to the Formation of Fluoranthene, a Non-Alternant Polycyclic Aromatic Hydrocarbon

Souvick Biswas, Sabrina Arias, Shane J. Goettl, Nureshan Dias, Stanislaw F. Wnuk, Musahid Ahmed,* Alexander M. Mebel,* and Ralf I. Kaiser*

Cite This: J. Am. Chem. Soc. 2026, 148, 45728−45737
Read Online
ACCESS | Metrics & More | Article Recommendations | Supporting Information

ABSTRACT: Nonalternant polycyclic aromatic hydrocarbons (PAHs) incorporating five-membered rings are fundamental intermediates linking planar aromatics to curved carbon nanostructures including fullerenes and nanotubes, yet their formation mechanisms are not fully understood. The detection of fluoranthene ($C_{16}H_{10}$) in samples from the near-Earth carbonaceous asteroid 162,173 Ryugu and 101,955 Bennu highlights the need for chemically viable pathways under both combustion and astrochemical conditions. Here, we demonstrate that fluoranthene forms efficiently commencing with barrierless recombination of resonance-stabilized indenyl ($C_9H_7^{\bullet}$) and benzyl ($C_7H_7^{\bullet}$) radicals. Microreactor experiments combined with electronic structure calculations reveal rapid carbon−carbon bond formation, cyclization, and dehydrogenation to the nonalternant framework. This mechanism represents an alternative to stepwise acetylene addition and enables early incorporation of pentagonal motifs during molecular growth. These findings establish radical−radical recombination as a versatile route to nonalternant PAHs, providing a unified framework for their formation in high-temperature combustion systems and carbon-rich astrophysical environments like circumstellar envelopes of carbon stars and planetary nebulae as their descendants.



INTRODUCTION

The recent detection of fluoranthene ($C_{16}H_{10}$) in pristine samples returned from the carbon-rich near-Earth asteroid 162,173 Ryugu by the *Hayabusa2* mission provides compelling evidence that structurally complex polycyclic aromatic hydrocarbons (PAHs) are indigenous components of primitive Solar System materials (Scheme 1).[1−4] These observations demonstrate that nonalternant PAHs such as fluorene ($C_{13}H_{10}$) and fluoranthene ($C_{16}H_{10}$), which incorporate five-membered rings within fused aromatic frameworks, can form and persist under extraterrestrial conditions. This observation implies that molecular processes operating in stellar outflows and interstellar clouds play a central role in shaping the organic inventory of planetesimals.[5−8] These pentagonal motifs are key structural elements that introduce geometric frustration into π-conjugated frameworks, enabling the transition from planar aromatic molecules to curved carbon architectures.[9−12] Fluoranthene ($C_{16}H_{10}$) occupies a pivotal position among PAHs, acting as a molecular bridge between planar aromatics and curved carbon nanostructures. Its carbon framework is also embedded in bowl-shaped intermediates such as corannulene ($C_{20}H_{10}$), which evolve into fullerene cages, including buckminsterfullerene (C_{60}), through bottom-up growth processes (Scheme 1).[13−17]

Despite its structural and astrochemical significance, the chemical pathways leading to fluoranthene remain incompletely understood. Current models of PAH growth in combustion and astrochemical environments are dominated by sequential ring-annulation mechanisms such as hydrogen abstraction−acetylene addition (HACA) and related pathways.[18−22] While early combustion models dictated that the HACA mechanism exclusively built six-membered aromatic frameworks, recent research has proven that HACA can also drive the formation of nonalternant, five-membered ring structures, such as acenaphthylene, depending on the starting radical precursor.[23−26] However, this structural divergence often introduces severe kinetic roadblocks, such as the third-ring cyclization barrier that halts traditional linear expansion.[27−29]

In this context, resonantly stabilized free radicals (RSFRs) offer an alternative framework for such aromatic growth.

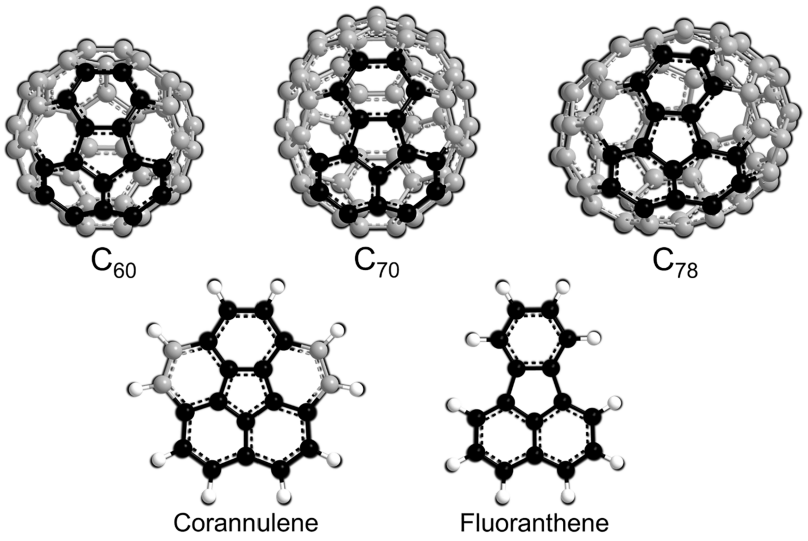
Received: June 27, 2026
Revised: September 27, 2026
Accepted: September 29, 2026
Published: October 12, 2026



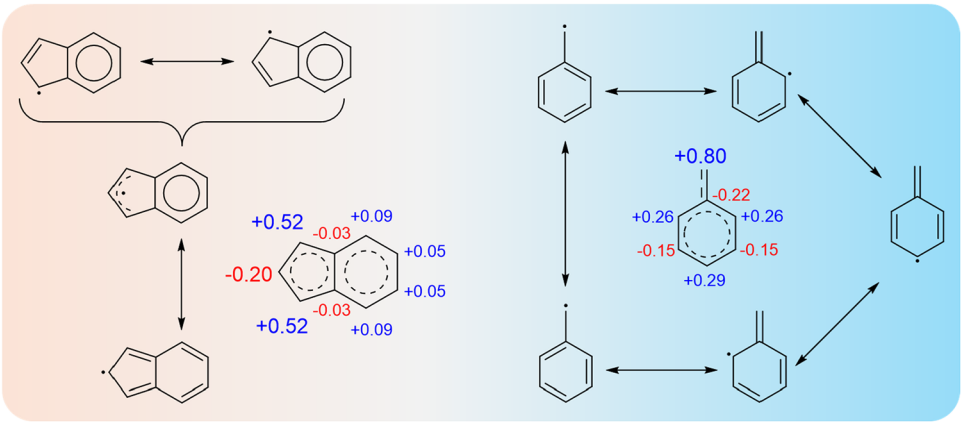
© 2026 American Chemical Society

https://doi.org/10.1021/jacs.6c13214
J. Am. Chem. Soc. 2026, 148, 45728−45737

Scheme 1. Central Role of the Fluoranthene Carbon Backbone (Black Atoms) in Buckminsterfullerene (C_{60}), Rugbyballene (C_{70}), and C_{78}-Fullerene along with Corannulene ($C_{20}H_{10}$)



Scheme 2. Spin Densities on the Carbon Centers of the Resonantly-Stabilized Indenyl ($C_9H_7^•$) and Benzyl ($C_7H_7^•$) Radicals Calculated at the ωB97X-D/6-311G Level of Theory**



Radicals such as benzyl ($C_7H_7^•$) and indenyl ($C_9H_7^•$) possess extensive delocalization of the unpaired electron across their π-systems (Scheme 2), conferring exceptional thermodynamic stability and relatively long lifetimes even under extreme thermal conditions.[30−35] These properties enable RSFRs to undergo barrierless or near-barrierless radical−radical recombination, facilitating rapid molecular mass growth without the repetitive steps required in HACA-type sequences.[31,36−42] Previous experimental and theoretical studies have demonstrated that RSFR-driven reactions can generate key PAH building blocks through unconventional pathways, including the formation of fluorene and related five-membered ring-containing structures.[29,39,43] Notably, indenyl-type radicals, which already contain a fused five-membered ring, provide a natural precursor for the formation of larger nonalternant PAHs.

Here, we combine experiment and theory to elucidate the formation of fluoranthene ($C_{16}H_{10}$), a prototypical nonalternant PAH, via recombination of the resonance-stabilized 1-indenyl ($C_9H_7^•$) and benzyl ($C_7H_7^•$) radicals. As a fundamental five-membered-ring-containing PAH, fluoranthene represents a key step toward the emergence of curved carbon frameworks in soot and fullerene-like carbonaceous matter. The radicals are generated *in situ* via selective carbon−bromine bond cleavage of helium-seeded 1-bromoindene (C_9H_7Br) and benzyl bromide (C_7H_7Br) precursors within a chemical microreactor. A short residence time of 100 μs restricts the chemistry to the earliest stages of molecular mass growth, thereby suppressing secondary growth reactions and enabling direct probing of fundamental bond-forming processes.[39,40,44] Electronic structure calculations reveal that fluoranthene formation proceeds at elevated temperatures through barrierless radical−radical cross-coupling, followed by H-loss/abstraction and ring-closure steps. This mechanism demonstrates how resonance-stabilized free radicals (RSFRs) can efficiently assemble five-membered-ring-containing PAHs while introducing curvature-inducing structural motifs at an early stage of molecular growth. Given the abundance of RSFRs in radical-rich environments, this chemistry is expected to operate in both combustion systems and circumstellar media, providing a common mechanistic route to nonalternant PAHs in terrestrial and extraterrestrial settings, including carbonaceous bodies such as the asteroid Ryugu.

https://doi.org/10.1021/jacs.6c13214
J. Am. Chem. Soc. 2026, 148, 45728−45737

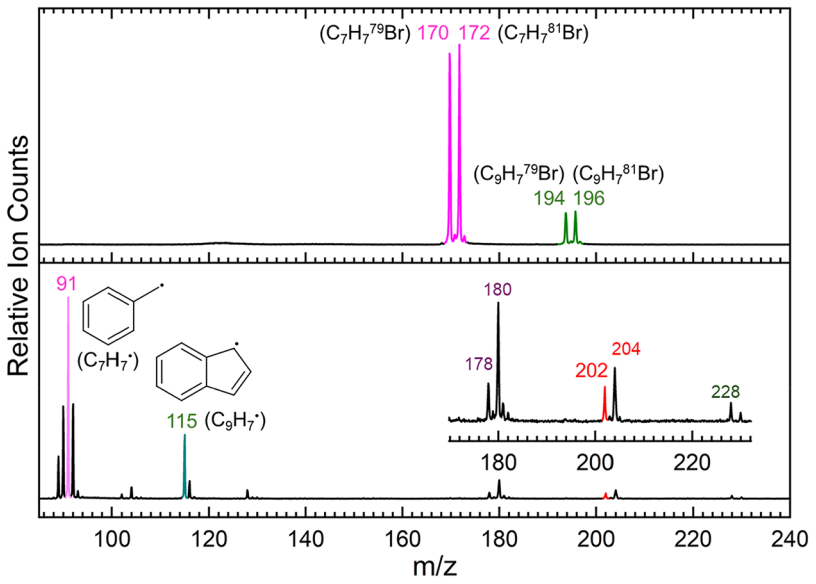


Figure 1. Photoionization mass spectra recorded at a photon energy of 9.50 eV for the precursors 1-bromoindene (C_9H_7Br) and benzyl bromide (C_7H_7Br) at 298 K (top) and the reactions of the indenyl ($C_9H_7^•$) plus benzyl radical ($C_7H_7^•$) at 1273 ± 20 K (bottom).

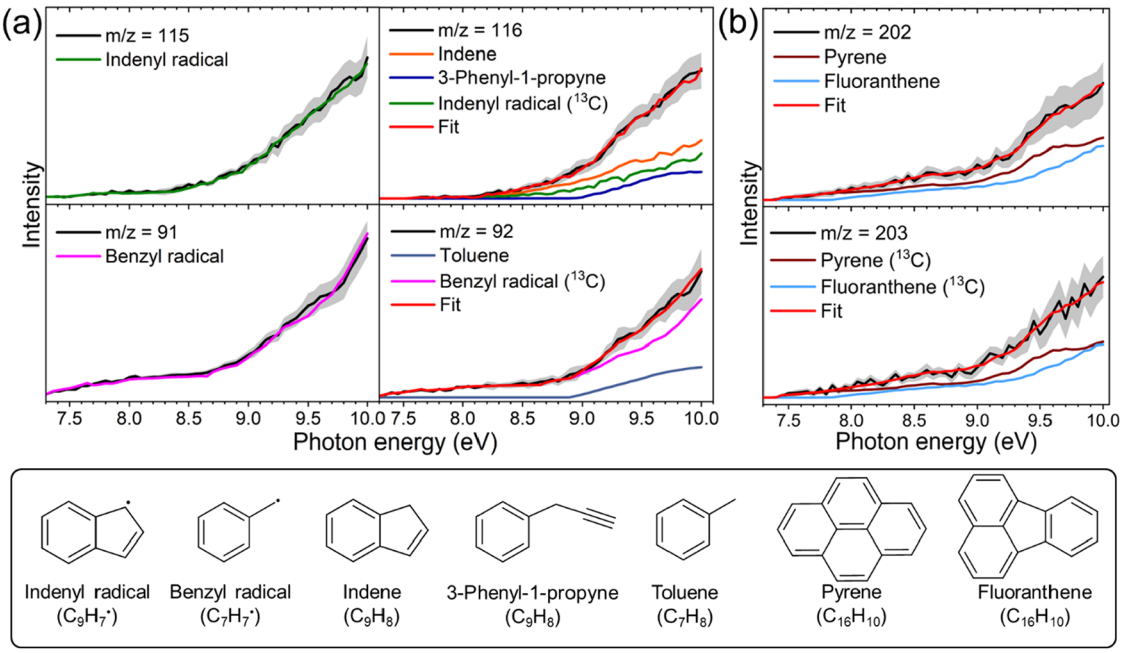


Figure 2. Photoionization efficiency (PIE) curves for mass-to-charge peaks at m/z = 91, 92, 115, 116, 202, and 203 along with the corresponding molecular formulas and structures. (a) Pyrolyzed products from the bromo-precursors including the key reactants indenyl ($C_9H_7^•$) and benzyl ($C_7H_7^•$). (b) Recombination products carrying the 16π-electron system at m/z = 202 ($C_{16}H_{10}$) and 203 ($^{13}C_{16}H_{10}$). Black: experimental PIE curves; green/orange/blue/magenta/brown/sky blue: reference PIE curves. In case of multiple contributions to one PIE curve, the red line resembles the overall fit. The error bars consist of two parts: ± 10% based on the accuracy of the photodiode and a 1-σ error of the PIE curve averaged over the individual scans.

■ RESULTS AND DISCUSSION

Mass Spectra and Photoionization Efficiency Curves

A representative mass spectrum recorded at a photon energy of 9.50 eV is displayed in Figure 1 for the recombination reaction between the 1-indenyl ($C_9H_7^•$; 115 amu) and benzyl radicals ($C_7H_7^•$; 91 amu) formed via flash pyrolysis of 1-bromoindene [$C_9H_7{}^{79}Br$ (194 amu), $C_9H_7{}^{81}Br$ (196 amu)] and benzyl bromide [$C_7H_7{}^{79}Br$ (170 amu), $C_7H_7{}^{81}Br$ (172 amu)], respectively. Alongside the primary radical reactants, multiple peaks appear at higher mass-to-charge ratios (m/z) as the result of distinct molecular mass growth processes. Major peaks at m/z = 92, 102, 104, 116, 128, 178, 180, 202, 204, 228, and 230 are identified (Figure 1, Figures S1−S3); these can be linked to hydrocarbons of the molecular formulas C_7H_8, C_8H_8, C_9H_8, $C_{10}H_8$, $C_{14}H_{10}$, $C_{14}H_{12}$, $C_{16}H_{10}$, $C_{16}H_{12}$, $C_{18}H_{12}$ and $C_{18}H_{14}$. For an isomer-specific assignment of these species, photoionization efficiency (PIE) curves are recorded at individual m/z peaks by scanning the photon energy in 0.05 eV steps in the range of 7.3 to 10.0 eV while simultaneously

https://doi.org/10.1021/jacs.6c13214
J. Am. Chem. Soc. 2026, 148, 45728−45737

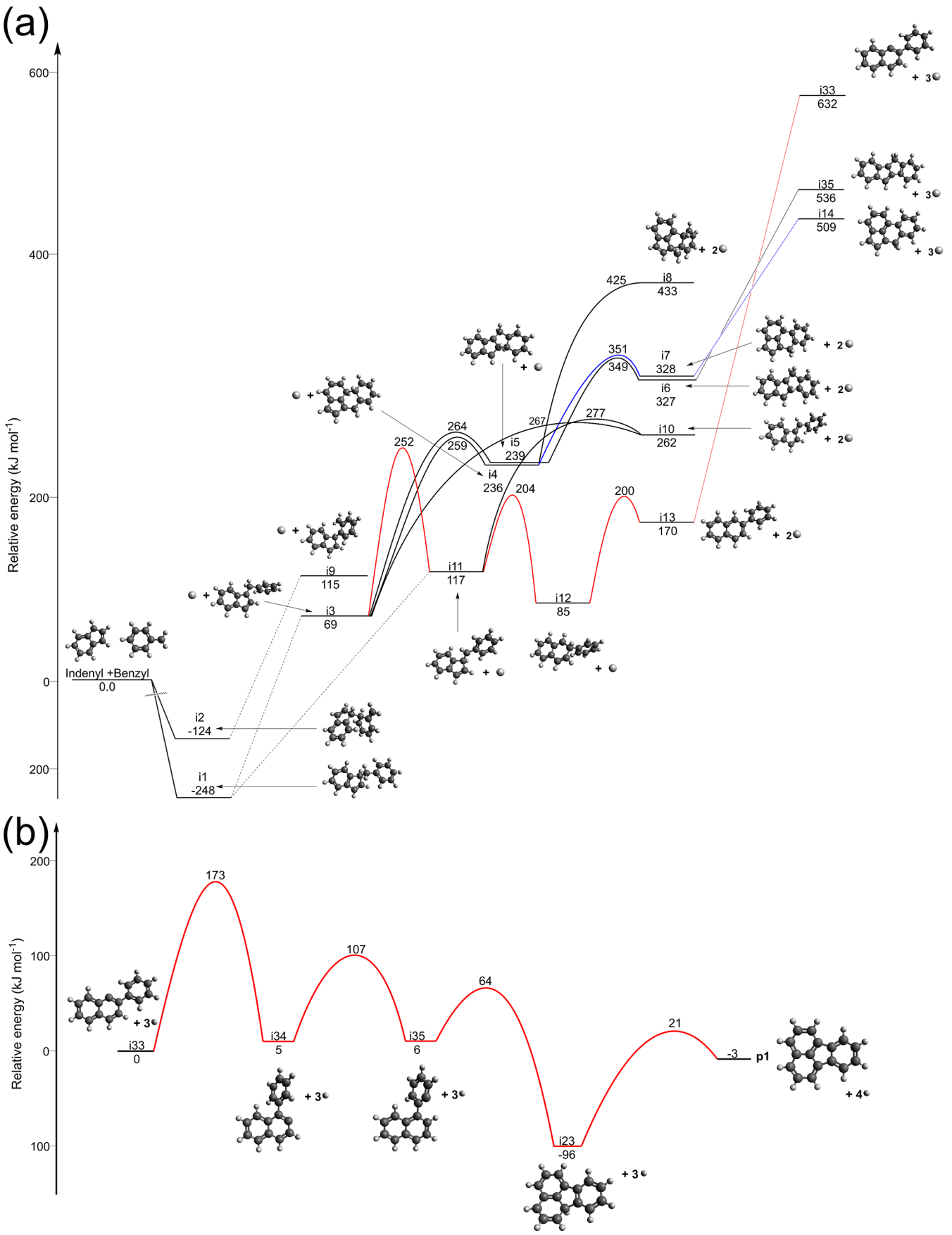


Figure 3. (a) Potential energy surface (PES) relevant to the formation of $C_{16}H_{11}^{\bullet}$ radical intermediates via the recombination of indenyl ($C_9H_7^{\bullet}$) and benzyl ($C_7H_7^{\bullet}$) radicals. (b) Formation route of fluoranthene ($C_{16}H_{10}$) from the **i33** ($C_{16}H_{11}^{\bullet}$) intermediate.

https://doi.org/10.1021/jacs.6c13214
J. Am. Chem. Soc. 2026, 148, 45728−45737

recording the ion count normalized to the photocurrent.[45−49] It is important to note that structural isomers, despite sharing the same formula, exhibit distinct PIE curves, enabling their identification.[42,50] PIE analysis shown in Figure 2 also confirms the primary radical reactants at m/z = 115 and 91 to be 1-indenyl ($C_9H_7^•$) and benzyl ($C_7H_7^•$) radicals, respectively.

The product signal at m/z = 230 represents the self-recombination adduct ($C_{18}H_{14}$) of 1-indenyl radicals ($C_9H_7^•$) (reaction 1), which eventually loses two hydrogen atoms in sequence to form $C_{18}H_{12}$ species (228 amu) via reaction 2.[51] Similarly, m/z = 180 ($C_{14}H_{12}$) may be attributed to the self-recombination of benzyl radicals ($C_7H_7^•$), followed by consecutive losses of two hydrogen atoms (reactions 3 and 4).[52] An analysis of the corresponding PIE curves at m/z = 228 and 180 reveals that they originate from chrysene and (*E*)-stilbene, respectively.

Most importantly, the reaction between 1-indenyl and benzyl radicals yields the $C_{16}H_{14}$ adduct via reaction 5, which subsequently undergoes successive hydrogen-atom losses and/or H atom abstractions by radicals such as H to form $C_{16}H_{12}$ (reaction 6). The latter species appears at m/z = 204 in the mass spectrum and its PIE fit indicates a major presence of 2-phenylnaphthalene alongside minor contribution from 1-phenylnaphthalene isomer (Figure S3). Further, upon sequential H atom loss, $C_{16}H_{10}$ (m/z = 202) is eventually formed (reaction 7).

$$C_9H_7^• \text{ (115 amu)} + C_9H_7^• \text{ (115 amu)} \rightarrow C_{18}H_{14} \text{ (230 amu)} \quad (1)$$

$$C_{18}H_{14} \text{ (230 amu)} \rightarrow C_{18}H_{12} \text{ (228 amu)} + 2H \text{ (1 amu)} \quad (2)$$

$$C_7H_7^• \text{ (91 amu)} + C_7H_7^• \text{ (91 amu)} \rightarrow C_{14}H_{14} \text{ (182 amu)} \quad (3)$$

$$C_{14}H_{14} \text{ (182 amu)} \rightarrow C_{14}H_{12} \text{ (180 amu)} + 2H \text{ (1 amu)} \quad (4)$$

$$C_9H_7^• \text{ (115 amu)} + C_7H_7^• \text{ (91 amu)} \rightarrow C_{16}H_{14} \text{ (206 amu)} \quad (5)$$

$$C_{16}H_{14} \text{ (206 amu)} \rightarrow C_{16}H_{12} \text{ (204 amu)} + 2H \text{ (1 amu)} \quad (6)$$

$$C_{16}H_{12} \text{ (204 amu)} \rightarrow C_{16}H_{10} \text{ (202 amu)} + 2H \text{ (1 amu)} \quad (7)$$

The recorded PIE curve at m/z = 202 displays an onset of ion counts at 7.40 ± 0.05 eV and an analysis (Figure 2b) reveals that this graph could be reproduced with the linear combination of the reference PIE curves for fluoranthene (sky blue; IE = 7.80 ± 0.05 eV) and pyrene (wine red; IE = 7.43 ± 0.05 eV). Further, the signal at m/z = 203 corresponds to the ^{13}C-substituted $^{13}CC_{15}H_{10}$ isotopologues of fluoranthene and pyrene at m/z = 202, with an overall abundance of approximately 18%, consistent with the natural abundance of ^{13}C (∼1.1%). Close comparison of the ionization threshold and the shape of the m/z = 203 PIE curve with those of the appropriately scaled m/z = 202 parent-ion curve confirms that no additional minor isomeric species contribute appreciably to the heavier mass channel. From the fitting of the m/z = 202 PIE curve and the reported photoionization cross sections (PICS) of fluoranthene and pyrene,[53] the relative contributions of the two isomers are estimated to be approximately 52% and 48%, respectively. Specifically, the reported PICS values at 8, 9, and 10 eV for each isomer were used to determine the corresponding contributions to the experimental PIE signal at these photon energies. The resulting ratios were then averaged over the three energies to minimize the influence of energy-dependent variations in the PICS and provide a robust estimate of the overall isomeric composition.

Having identified m/z = 202 and 203 as the result of molecular mass growth processes due to the indenyl-benzyl recombination reaction, we also briefly discuss the origin of ion counts in the range of 92−180 amu. Since the 1-indenyl and benzyl radicals can undergo pyrolysis in the chemical microreactor, they may decompose into smaller hydrocarbon fragments such as propargyl ($C_3H_3^•$), cyclopentadienyl ($C_5H_5^•$), phenyl ($C_6H_5^•$), benzene (C_6H_6) and acetylene (C_2H_2).[47,54,55] Reactions of these fragments with the parent radicals (Figure S2, Table S1, Supporting Information S2) likely contribute to the ion signals observed over the m/z 92−180 range.[47,56]

Reaction Mechanism

With experimental evidence for the formation of fluoranthene ($C_{16}H_{10}$) through the recombination of the 1-indenyl ($C_9H_7^•$) with benzyl ($C_7H_7^•$) radicals, we now seek to decipher the underlying reaction mechanisms (Figure 3) by performing electronic structure calculations of the relevant potential energy surfaces (PES). These calculations were conducted at the G3(CC,MP2)//ωB97X-D/6−311G** level of theory with the reaction network from the indenyl-benzyl radical recombination presented in Figures 3 and S4. Initially, the reactant radicals barrierlessly recombine at the sp^2 carbon radical centers holding highest spin densities to form the energetically most stable adduct, 1-benzyl-1*H*-indene ($C_{16}H_{14}$; **i1**)−bound by 248 kJ mol^{-1} with respect to the separated reactants. An endoergic hydrogen atom loss (317 kJ mol^{-1}) from the C1-center of indenyl moiety in **i1** yields **i3** ($C_{16}H_{13}^•$). The prevailing mechanism of isomerization and decomposition of **i3** involves H atom migration from the CH_2 group to the neighboring carbon atom in the five-membered ring of the indenyl moiety followed by extension of the five-membered ring into a six-membered one via CH insertion and completed by an H atom loss forming 2-phenylnaphthalene **i13**. The overall **i3** → **i13** + H reaction is endoergic by 101 kJ mol^{-1}, with the highest barrier for the H migration step being 183 kJ mol^{-1} relative to **i3**. The only other competitive pathway is H atom loss from the CH_2 group forming **i10** via a barrier of 198 kJ mol^{-1}; **i10** lies 92 kJ mol^{-1} higher in energy than **i13**. RRKM-Master Equation (RRKM-ME) calculations at the experimental temperature and pressure of 0.1 atm characteristic for the hot zone in the microreactor results in the **i10**/**i13** branching ratio as 56/44, however, **i10** can be efficiently converted to the significantly more stable $C_{16}H_{12}$ isomer (**i13**) by H-assisted isomerization. Thus, the calculations predict 2-phenyl-naphthalene **i13** to be not only the most energetically favorable but also kinetically prevailing $C_{16}H_{12}$ species under the experimental conditions, which is corroborated by the experimental identification from the fitted PIE curve at m/z = 204 (Figure S3).

Most important, **i13** eventually generates the experimentally detected fluoranthene (**p1**). The pathway begins from the H loss in the naphthalene moiety from the *ortho* position with respect to phenyl endoergic by 462 kJ mol^{-1} producing

https://doi.org/10.1021/jacs.6c13214
J. Am. Chem. Soc. 2026, 148, 45728−45737

$C_{16}H_{11}^{\bullet}$ (**i33**). With a high abundance of H atoms in the microreactor produced at the previous steps, it is likely that **i33** forms through direct H abstraction, **i13** + H → **i33** + H_2, with the endoergicity being reduced to 30 kJ mol^{-1} owing to the formation of an H−H bond. The barriers (~68 kJ mol^{-1}) and rapid reaction kinetics of direct H abstraction from PAHs are well established in the literature.[57] Next, **i33** can efficiently rearrange and lose atomic hydrogen forming **p1**. This pathway involves migration of the phenyl ring from β to α position in the naphthalene moiety producing **i34** via a barrier of 173 kJ mol^{-1}, 1,4-H shift from phenyl to the β position in naphthalene via a barrier of 102 kJ mol^{-1} to **i35**, closure of the five-membered ring occurring by rotation of the phenyl group leading to **i23** with a barrier of 58 kJ mol^{-1}, and finally, H loss to fluoranthene over a barrier of 117 kJ mol^{-1}. Overall, the $C_{16}H_{11}^{\bullet}$ (**i33**) → **i34** → **i35** → **i23** → $C_{16}H_{10}$ (**p1**) + H reaction is slightly exoergic (−3 kJ mol^{-1}) and features the highest barrier of 173 kJ mol^{-1} for the first phenyl migration step. Starting from **i34**, the reaction mechanism is reminiscent of the phenyl addition and dehydrocyclization (PAC) mechanism discovered earlier for the formation of fluoranthene in the phenyl + naphthalene reaction.[58] RRKM-ME calculations of product branching ratios show that **i33** is exclusively converted to **p1** + H at temperatures above 1000 K. Summarizing the entire reaction sequence, the indenyl + benzyl → fluoranthene + 4H reaction is 629 kJ mol^{-1} endoergic. However, if the energy-demanding reaction steps of H loss from the closed-shell $C_{16}H_{14}$ and $C_{16}H_{12}$ molecules occur via direct H abstraction by H via the following mechanism, the overall reaction would be 235 kJ mol^{-1} exoergic. In this mechanism, the reaction is catalyzed by H atoms, which could be initially formed via the 69 kJ mol^{-1} endoergic well-skipping mechanism of the formation of **i3**, $C_9H_7^{\bullet}$ + $C_7H_7^{\bullet}$ → $C_{16}H_{13}^{\bullet}$ (**i3**) + H, or via thermal decomposition of **i1**. The rate-determining steps in the H-catalyzed mechanism involve the reactions on the $C_{16}H_{13}^{\bullet}$ and $C_{16}H_{11}^{\bullet}$ potential energy surfaces, which exhibit the highest barriers of 183 and 173 kJ mol^{-1}, with respect to the initial intermediates **i3** and **i33**, respectively. Such barriers can be readily overcome at high temperatures. In particular, at the experimental temperature the RRKM-ME computed rate constants for the formation of **i13** + H from **i3** and **p1** + H from **i33** are 5×10^4 and 7×10^5 s^{-1}, respectively, indicating that these reactions can be completed in a few tens of microseconds. Nonetheless, the underlying conversion of 2-phenylnaphthalene (**i13**) to fluoranthene warrants an independent experimental investigation under identical reaction conditions in future work. Such a study could provide deeper insight into the reaction network, including radical isomerization efficiencies, branching ratios among competing product channels, and the associated kinetic parameters. However, a comprehensive investigation of this nature is beyond the scope of the present study.

$C_9H_7^{\bullet} + C_7H_7^{\bullet} \rightarrow C_{16}H_{14}$ (**i1**)

$C_{16}H_{14}$ (**i1**) + H → $C_{16}H_{13}^{\bullet}$ (**i3**) + H_2

$C_{16}H_{13}^{\bullet}$ (**i3**) → **i3** → **i11** → **i12** → $C_{16}H_{12}$ (**i13**) + H

$C_{16}H_{12}$ (**i13**) + H → $C_{16}H_{11}^{\bullet}$ (**i33**) + H_2

$C_{16}H_{11}^{\bullet}$ (**i33**) → **i34** → **i35** → **i23** → $C_{16}H_{10}$ (**p1**) + H

$C_9H_7^{\bullet} + C_7H_7^{\bullet}$ + H → $C_{16}H_{10}$ (**p1**) + $2H_2$ + H

We now address the possible formation of minor $C_{16}H_{10}$ products, such as pyrene (**p3**) detected experimentally and acephenanthrylene (**p2**)—see Figure S5. Since fluoranthene is the dominant $C_{16}H_{10}$ product which forms on a microsecond scale, it is plausible that **p1** can be converted to other $C_{16}H_{10}$ species via H-assisted isomerization, **p1** + H → **p2**/**p3** + H. In fact, the pathway to acephenanthrylene, **p1** + H → **i22** → **i21** → **i20** → **i14** → **p2** + H, involves H addition to a six-membered ring in fluoranthene followed by the 'methylene walk' mechanism, in which the six-membered ring is contracted to a five-membered one by expulsion of the CH_2 group and the latter inserts in the central five-membered-ring and expands it to a six-membered ring.[59] The methylene walk essentially switches positions of the six- and five-membered rings in fluoranthene eventually leading to acephenanthrylene after an H atom loss. The highest in energy transition state on the **p1** + H → **p2** + H pathway is located 92 kJ mol^{-1} above **p1** + H. The pathway to pyrene, **p1** + H (→ **i23**) → **i24** → **i36** → **i37** → **i38** → **p3** + H, is somewhat more complex and energy demanding. From **i24**, it proceeds by an exchange of positions of the five- and six-membered rings moving the five-membered ring to a peripheral position in **i36** followed by a ring flip involving opening of the five-membered ring, rotation of the CHCHCHCH group and closure of a six-membered ring in **i38**, with the reaction being completed by an atomic hydrogen loss from the latter. Although the H-assisted production of pyrene from fluoranthene is 59 kJ mol^{-1} exoergic, the pathway involves the highest barrier of 129 kJ mol^{-1} and is kinetically unfavorable as compared to the H-assisted isomerization to acephenanthrylene. The calculated branching ratios of **p2** and **p3** under the experimental conditions are 78% and 14%, respectively. Although the experimental identification of acephenanthrylene is limited by the lack of an available PIE reference curve, its calculated adiabatic ionization energy of 7.71 eV (**p2**) suggests that it may contribute to the observed PIE signal at m/z = 202. Nevertheless, the computed reaction mechanism and kinetic analysis unequivocally show that fluoranthene is the predominant $C_{16}H_{10}$ product of the 1-indenyl + benzyl reaction. The experimentally observed larger share of pyrene than the computed value may be attributed to secondary reaction channels stemming from detected minor products, for instance, phenanthrene upon H atom loss can combine with acetylene via a low barrier (20 kJ mol^{-1}) HACA process,[60] with a subsequent H atom loss resulting in pyrene, whereas phenanthrene can be formed as a prevailing product in the benzyl radical self-recombination reaction[52] and acetylene may stem, e.g., from unimolecular decomposition of either indenyl[61,62] or benzyl.[63]

The temperature of interest for the growth of PAHs within the shocked inner wind zone of the IRC+10216 circumstellar envelope is between 900 and 1100 K.[64] The calculated rate constant for the C_9H_7 + C_7H_7 reaction strongly depends on temperature and pressure (Figure S6). For instance, at the experimental temperature in the pressure range of 0.01−0.1 atm typical for the reactive zone of the microreactor, the calculated rate constant is in the range of $1.4-5.7 \times 10^{-12}$ cm^3 $molecule^{-1}$ s^{-1}, with the prevailing product (>99%) being the thermalized **i1** ($C_{16}H_{14}$) species. The rate constant for the well-skipping pathway forming **i3** ($C_{16}H_{13}$) is only 1.1×10^{-14} cm^3 $molecule^{-1}$ s^{-1} under these conditions. In the IRC+10216 circumstellar envelope at 1000 K, the rate constant and the reaction outcome is ultimately determined by the pressure; at pressures under 4×10^{-7} atm, collisional stabilization of **i1**

https://doi.org/10.1021/jacs.6c13214
J. Am. Chem. Soc. 2026, 148, 45728−45737

does not occur and the reaction produces nearly exclusively **i3** + H with a low rate constant of 1.25×10^{-15} cm^3 molecule^{-1} s^{-1}. With rising pressure, the channel forming collisionally stabilized **i1** steadily takes over, with its rate constant increasing to $\sim 10^{-12}$ cm^3 molecule^{-1} s^{-1} at $p = 10^{-4}$ atm. For comparison, in the limit of zero pressure, the rate constant to form pyrene via the HACA mechanism in the phenanthrenyl + C_2H_2 reaction is 8.4×10^{-14} cm^3 molecule^{-1} s^{-1}, whereas under the microreactor conditions in the present experiment, its value increases to 4.4×10^{-13} cm^3 molecule^{-1} s^{-1}.[27] However, the direct comparison of the radical recombination and HACA rate constants is not informative, as the overall mechanism additionally involves H abstraction and radical decomposition steps. The competition between various mechanisms of PAH growth depends on the conditions and abundances of other species involved, such as, e.g., the concentration of H atoms (from 10^{12}–10^{14} cm^{-3} under microreactor conditions[65,66] to 10^{14}–10^{15} cm^{-3} in sooting flames[67] or to much lower values in circumstellar envelopes). Although the present study does not focus on a detailed kinetic modeling under these particular reaction conditions, a comprehensive investigation incorporating the relevant reaction network, species concentrations, and associated rate coefficients represents an important direction for future work to assess the relative importance of the competing PAH growth mechanisms.

CONCLUSIONS

In summary, the above findings reveal a previously unrecognized high-temperature route to the formation of nonalternant aromatic ring systems, providing new molecular-level insight into the chemistry operating in carbon-rich circumstellar environments such as IRC+10216 and related stellar outflows.[68,69] The widespread occurrence of fluoranthene in carbonaceous meteorites and asteroid samples such as Ryugu and Bennu points to an efficient and likely universal formation route, which is rationalized here through *endoergic* pathways accessible under thermally extreme conditions.[70−73] Central to this work is the discovery of a barrierless radical−radical recombination between the resonance-stabilized indenyl and benzyl radicals. Stabilized by 248 kJ mol^{-1}, the resulting adduct undergoes *cyclization*, *dehydrogenation*, and *ring-rearrangement* to form fluoranthene. This pathway constitutes a kinetically competitive route that bypasses conventional multistep ring-annulation mechanisms and directly introduces a five-membered ring at the C_{16} stage, generating an intrinsically nonalternant aromatic framework. Although fluoranthene itself is planar, following two HACA steps, it can readily produce a nonplanar bowl-shaped corannulene molecules, $C_{20}H_{10}$.[43] The early incorporation of five-membered rings introduces molecular curvature at comparatively small sizes, potentially reshaping nucleation pathways beyond those predicted by purely benzenoid growth models and facilitates a structurally efficient entry point toward bowl-shaped PAHs and fullerene precursors—consistent with nanometer-scale, disordered aromatic domains observed in primitive Solar System materials.[1−3,72,74,75] Given its finite dipole moment (0.34 D), fluoranthene is a promising candidate for direct gas-phase detection in the interstellar medium through rotational spectroscopy with the Atacama Large Millimeter/submillimeter Array (ALMA), offering constraints on the origin and evolution of cosmic carbonaceous matter.[76] The barriers featured in the depicted PES can be readily overcome in inner circumstellar regions where temperatures approach several thousand Kelvin, especially if the reactions are assisted by direct H abstractions, enabling fluoranthene formation under astrophysically relevant conditions. The mechanism establishes a direct chemical connection between circumstellar PAH formation and meteoritic organic matter, offering a plausible origin for the remarkable abundance and diversity of PAHs detected in Ryugu.[3,72,74,77] By demonstrating how small resonance-stabilized radicals can seed the formation of intrinsically curved carbon frameworks, this work establishes radical−radical recombination as a fundamental pathway in the chemical evolution of carbon throughout the Galaxy.

ASSOCIATED CONTENT

Data Availability Statement

The data that support the findings of this study are available from the corresponding author upon reasonable request.

Supporting Information

The Supporting Information is available free of charge at https://pubs.acs.org/doi/10.1021/jacs.6c13214.

Experimental and computational methods; complete mass spectra; additional PIE curves for peaks in the range m/z = 102−230; tentative PIE curve fitting for possible products at m/z = 204; list of all mass-growth products and brief description of their formation path; full potential energy surface and formation routes of acephenanthrylene, pyrene, and phenanthrenyl + acetylene; calculated rate constants for different product channels of the C_9H_7 + C_7H_7 reaction as a function of temperature and pressure individually; rate constants and product branching ratios for the reaction on the $C_{16}H_{13}$ and $C_{16}H_{11}$ potential energy surfaces; coordinates of the reactants, products, intermediates and transition states (PDF)

AUTHOR INFORMATION

Corresponding Authors

Musahid Ahmed − *Chemical Sciences Division, Lawrence Berkeley National Laboratory, Berkeley, California 94720, United States;* orcid.org/0000-0003-1216-673X; Email: mahmed@lbl.gov

Alexander M. Mebel − *Department of Chemistry and Biochemistry, Florida International University, Miami, Florida 33199, United States;* orcid.org/0000-0002-7233-3133; Email: mebela@fiu.edu

Ralf I. Kaiser − *Department of Chemistry, University of Hawai'i at Manoa, Honolulu, Hawaii 96822, United States;* orcid.org/0000-0002-7233-7206; Email: ralfk@hawaii.edu

Authors

Souvick Biswas − *Department of Chemistry, University of Hawai'i at Manoa, Honolulu, Hawaii 96822, United States;* Present Address: School of Chemistry, Indian Institute of Science Education and Research Thiruvananthapuram (IISER TVM), Thiruvananthapuram 695551, India; orcid.org/0000-0002-1643-2663

Sabrina Arias − *Department of Chemistry and Biochemistry, Florida International University, Miami, Florida 33199, United States*

Shane J. Goettl − *Department of Chemistry, University of Hawai'i at Manoa, Honolulu, Hawaii 96822, United States;* orcid.org/0000-0003-1796-5725

Nureshan Dias − *Chemical Sciences Division, Lawrence Berkeley National Laboratory, Berkeley, California 94720, United States*

Stanislaw F. Wnuk − *Department of Chemistry and Biochemistry, Florida International University, Miami, Florida 33199, United States;* orcid.org/0000-0002-3111-3919

Complete contact information is available at: https://pubs.acs.org/10.1021/jacs.6c13214

Notes

The authors declare no competing financial interest.

■ ACKNOWLEDGMENTS

This work was supported by the US Department of Energy, Basic Energy Sciences DE-FG02-03ER15411 (experimental studies). N.D. and M.A. were supported by the Director, Office of Science, Office of Basic Energy Sciences, of the U.S. Department of Energy under Contract No. DE-AC02-05CH11231, through the Gas Phase Chemical Physics program of the Chemical Sciences Division. The Advanced Light Source at Berkeley is also supported under Contract No. DE-AC02-05CH11231.

■ REFERENCES

(1) Yada, T.; Abe, M.; Okada, T.; Nakato, A.; Yogata, K.; Miyazaki, A.; Hatakeda, K.; Kumagai, K.; Nishimura, M.; Hitomi, Y.; et al. Preliminary Analysis of the Hayabusa2 Samples Returned from C-type Asteroid Ryugu. *Nat. Astron.* **2022**, *6*, 214−220.

(2) Yokoyama, T.; Nagashima, K.; Nakai, I.; Young, E. D.; Abe, Y.; Aléon, J.; Alexander, C. M. O. D.; Amari, S.; Amelin, Y.; Bajo, K.-i.; et al. Samples Returned from the Asteroid Ryugu are Similar to Ivuna-type Carbonaceous Meteorites. *Science* **2022**, *379*, No. eabn7850.

(3) Naraoka, H.; Takano, Y.; Dworkin, J. P.; Oba, Y.; Hamase, K.; Furusho, A.; Ogawa, N. O.; Hashiguchi, M.; Fukushima, K.; Aoki, D.; et al. Soluble Organic Molecules in Samples of the Carbonaceous Asteroid (162173) Ryugu. *Science* **2023**, *379*, No. eabn9033.

(4) Oba, Y.; Takano, Y.; Dworkin, J. P.; Naraoka, H. Ryugu Asteroid Sample Return Provides a Natural Laboratory for Primordial Chemical Evolution. *Nat. Commun.* **2023**, *14*, No. 3107.

(5) Tielens, A. G. G. M. Interstellar Polycyclic Aromatic Hydrocarbon Molecules. *Annu. Rev. Astron. Astrophys.* **2008**, *46*, 289−337.

(6) Allamandola, L. J.; Tielens, A. G. G. M.; Barker, J. R. Polycyclic Aromatic Hydrocarbons and the Unidentified Infrared Emission Bands: Auto Exhaust along the Milky Way. *Astrophys. J.* **1985**, *290*, L25−L28.

(7) Ehrenfreund, P.; Charnley, S. B. Organic Molecules in the Interstellar Medium, Comets, and Meteorites: A Voyage from Dark Clouds to the Early Earth. *Annu. Rev. Astron. Astrophys.* **2000**, *38*, 427−483.

(8) Herbst, E.; van Dishoeck, E. F. Complex Organic Interstellar Molecules. *Annu. Rev. Astron. Astrophys.* **2009**, *47*, 427−480.

(9) Kroto, H. W.; Heath, J. R.; O'Brien, S. C.; Curl, R. F.; Smalley, R. E. C60: Buckminsterfullerene. *Nature* **1985**, *318*, 162−163.

(10) Dunk, P. W.; Kaiser, N. K.; Hendrickson, C. L.; Quinn, J. P.; Ewels, C. P.; Nakanishi, Y.; Sasaki, Y.; Shinohara, H.; Marshall, A. G.; Kroto, H. W. Closed Network Growth of Fullerenes. *Nat. Commun.* **2012**, *3*, No. 855.

(11) Parker, D. S. N.; Zhang, F.; Kim, Y. S.; Kaiser, R. I.; Landera, A.; Kislov, V. V.; Mebel, A. M.; Tielens, A. G. G. M. Low Temperature Formation of Naphthalene and its Role in the Synthesis of PAHs (Polycyclic Aromatic Hydrocarbons) in the Interstellar Medium. *Proc. Natl. Acad. Sci. U.S.A.* **2012**, *109*, 53−58.

(12) Zhen, J.; Castellanos, P.; Paardekooper, D. M.; Linnartz, H.; Tielens, A. G. G. M. Laboratory Formation of Fullerenes from PAHs: Top-down Interstellar Chemistry. *Astrophys. J. Lett.* **2014**, *797*, No. L30.

(13) Scott, L. T. Methods for the Chemical Synthesis of Fullerenes. *Angew. Chem., Int. Ed.* **2004**, *43*, 4994−5007.

(14) Irle, S.; Zheng, G.; Wang, Z.; Morokuma, K. The C60 Formation Puzzle "Solved": QM/MD Simulations Reveal the Shrinking Hot Giant Road of the Dynamic Fullerene Self-Assembly Mechanism. *J. Phys. Chem. B* **2006**, *110*, 14531−14545.

(15) Nestoros, E.; Stuparu, M. C. Corannulene: A Molecular Bowl of Carbon with Multifaceted Properties and Diverse Applications. *Chem. Commun.* **2018**, *54*, 6503−6519.

(16) Frenklach, M. Reaction Mechanism of Soot Formation in Flames. *Phys. Chem. Chem. Phys.* **2002**, *4*, 2028−2037.

(17) Frenklach, M.; Feigelson, E. D. Formation of Polycyclic Aromatic Hydrocarbons in Circumstellar Envelopes. *Astrophys. J.* **1989**, *341*, 372−384.

(18) Wang, H.; Frenklach, M. A detailed Kinetic Modeling Study of Aromatics Formation in Laminar Premixed Acetylene and Ethylene Flames. *Combust. Flame* **1997**, *110*, 173−221.

(19) Richter, H.; Howard, J. B. Formation of Polycyclic Aromatic Hydrocarbons and Their Growth to Soot—A Review of Chemical Reaction Pathways. *Prog. Energy Combust. Sci.* **2000**, *26*, 565−608.

(20) Altarawneh, M.; Ali, L. Formation of Polycyclic Aromatic Hydrocarbons (PAHs) in Thermal Systems: A Comprehensive Mechanistic Review. *Energy Fuels* **2024**, *38* (22), 21735−21792.

(21) Yang, T.; Troy, T. P.; Xu, B.; Kostko, O.; Ahmed, M.; Mebel, A. M.; Kaiser, R. I. Hydrogen-Abstraction/Acetylene-Addition Exposed. *Angew. Chem., Int. Ed.* **2016**, *55*, 14983−14987.

(22) Zhao, L.; Xu, B.; Ablikim, U.; Lu, W.; Ahmed, M.; Evseev, M. M.; Bashkirov, E. K.; Azyazov, V. N.; Howlader, A. H.; Wnuk, S. F.; Mebel, A. M.; Kaiser, R. I. Gas-Phase Synthesis of Triphenylene ($C_{18}H_{12}$). *ChemPhysChem* **2019**, *20*, 791−797.

(23) Frenklach, M.; Jasper, A. W.; Mebel, A. M. Phenalenyl Growth Reactions and Implications for Prenucleation Chemistry of Aromatics in Flames. *Phys. Chem. Chem. Phys.* **2024**, *26*, 13034−13048.

(24) Kislov, V. V.; Sadovnikov, A. I.; Mebel, A. M. Formation Mechanism of Polycyclic Aromatic Hydrocarbons beyond the Second Aromatic Ring. *J. Phys. Chem. A* **2013**, *117*, 4794−4816.

(25) Reizer, E.; Viskolcz, B.; Fiser, B. Formation and Growth Mechanisms of Polycyclic Aromatic Hydrocarbons: A Mini-review. *Chemosphere* **2022**, *291*, No. 132793.

(26) Johansson, K. O.; Head-Gordon, M. P.; Schrader, P. E.; Wilson, K. R.; Michelsen, H. A. Resonance-stabilized Hydrocarbon-Radical Chain Reactions May Explain Soot Inception and Growth. *Science* **2018**, *361*, 997−1000.

(27) Frenklach, M.; Singh, R. I.; Mebel, A. M. On the Low-Temperature Limit of HACA. *Proc. Combust. Inst.* **2019**, *37*, 969−976.

(28) Mebel, A. M.; Georgievskii, Y.; Jasper, A. W.; Klippenstein, S. J. Temperature- and Pressure-Dependent Rate Coefficients for the HACA Pathways from Benzene to Naphthalene. *Proc. Combust. Inst.* **2017**, *36*, 919−926.

(29) Parker, D. S. N.; Kaiser, R. I.; Bandyopadhyay, B.; Kostko, O.; Troy, T. P.; Ahmed, M. Unexpected Chemistry from the Reaction of Naphthyl and Acetylene at Combustion-Like Temperatures. *Angew. Chem., Int. Ed.* **2015**, *54*, 5421−5424.

(30) Yang, Z.; Galimova, G. R.; He, C.; Goettl, S. J.; Paul, D.; Lu, W.; Ahmed, M.; Mebel, A. M.; Li, X.; Kaiser, R. I. Gas-phase Formation of the Resonantly Stabilized 1-Indenyl ($C_9H_7^{\bullet}$) Radical in the Interstellar Medium. *Sci. Adv.* **2023**, *9*, No. eadi5060.

(31) Kaiser, R. I.; Zhao, L.; Lu, W.; Ahmed, M.; Zagidullin, M. V.; Azyazov, V. N.; Mebel, A. M. Formation of Benzene and Naphthalene through Cyclopentadienyl-Mediated Radical−Radical Reactions. *J. Phys. Chem. Lett.* **2022**, *13*, 208−213.

(32) Zhao, L.; Kaiser, R. I.; Lu, W.; Ahmed, M.; Oleinikov, A. D.; Azyazov, V. N.; Mebel, A. M.; Howlader, A. H.; Wnuk, S. F. Gas

Phase Formation of Phenalene via 10π-Aromatic, Resonantly Stabilized Free Radical Intermediates. *Phys. Chem. Chem. Phys.* **2020**, *22*, 15381−15388.
(33) Dellinger, B.; Lomnicki, S.; Khachatryan, L.; Maskos, Z.; Hall, R. W.; Adounkpe, J.; McFerrin, C.; Truong, H. Formation and Stabilization of Persistent Free Radicals. *Proc. Combust. Inst.* **2007**, *31*, 521−528.
(34) Li, W.; Wu, M.; Wang, C.; Huang, J.; Yang, J.; Xu, M.; Zhang, F.; Yang, T.; Zhao, L. Unconventional Pathway for the Gas-Phase Formation of 14π-PAHs via Self-Reaction of the Resonantly Stabilized Radical Fulvenallenyl ($C_7H_5^{\cdot}$). *Chem. Sci.* **2025**, *16*, 7864−7875.
(35) Sinha, S.; Rahman, R. K.; Raj, A. On the Role of Resonantly Stabilized Radicals in Polycyclic Aromatic Hydrocarbon (PAH) Formation: Pyrene And Fluoranthene Formation From Benzyl−Indenyl Addition. *Phys. Chem. Chem. Phys.* **2017**, *19*, 19262−19278.
(36) Zhao, L.; Kaiser, R. I.; Lu, W.; Xu, B.; Ahmed, M.; Morozov, A. N.; Mebel, A. M.; Howlader, A. H.; Wnuk, S. F. Molecular Mass Growth through Ring Expansion in Polycyclic Aromatic Hydrocarbons via Radical−Radical Reactions. *Nat. Commun.* **2019**, *10*, No. 3689.
(37) Gao, J.; Li, Y.; Shang, Y.; Liu, Y.; Liu, B.; Guan, J.; Wang, Z.; Hu, Y. Propargyl ($\bullet C_3H_3$) and Butadienyl ($\bullet$i-C_4H_5) Radical−Radical Reactions Well-Skipping to Vinylcyclopentadienyl Radical and Toluene: A Theoretical and Kinetic Modeling Study. *J. Chem. Phys.* **2025**, *163*, No. 094303.
(38) Zhao, L.; Lu, W.; Ahmed, M.; Zagidullin, M. V.; Azyazov, V. N.; Morozov, A. N.; Mebel, A. M.; Kaiser, R. I. Gas-phase Synthesis of Benzene via the Propargyl Radical Self-reaction. *Sci. Adv.* **2021**, *7*, No. eabf0360.
(39) He, C.; Kaiser, R. I.; Lu, W.; Ahmed, M.; Pivovarov, P. S.; Kuznetsov, O. V.; Zagidullin, M. V.; Mebel, A. M. Unconventional Pathway in the Gas-Phase Synthesis of 9H-Fluorene (C13H10) via the Radical−Radical Reaction of Benzyl (C7H7) with Phenyl (C6H5). *Angew. Chem., Int. Ed.* **2023**, *62*, No. e202216972.
(40) He, C.; Kaiser, R. I.; Lu, W.; Ahmed, M.; Reyes, Y.; Wnuk, S. F.; Mebel, A. M. Exotic Reaction Dynamics in the Gas-Phase Preparation of Anthracene ($C_{14}H_{10}$) via Spiroaromatic Radical Transients in the Indenyl−Cyclopentadienyl Radical−Radical Reaction. *J. Am. Chem. Soc.* **2023**, *145*, 3084−3091.
(41) Goettl, S. J.; Turner, A. M.; Krasnoukhov, V. S.; Azyazov, V. N.; Kanayama, K.; Hemberger, P.; Mebel, A. M.; Kaiser, R. I. Gas-phase Synthesis of Anthracene and Phenanthrene via Radical-Radical Reaction Induced Ring Expansions. *Sci. Adv.* **2025**, *11*, No. eadv0692.
(42) Kaiser, R. I.; Hansen, N. An Aromatic Universe−A Physical Chemistry Perspective. *J. Phys. Chem. A* **2021**, *125*, 3826−3840.
(43) Zhao, L.; Doddipatla, S.; Kaiser, R. I.; Lu, W.; Kostko, O.; Ahmed, M.; Tuli, L. B.; Morozov, A. N.; Howlader, A. H.; Wnuk, S. F.; Mebel, A. M.; Azyazov, V. N.; Mohamed, R. K.; Fischer, F. R. Gas-phase Synthesis of Corannulene − A Molecular Building Block of Fullerenes. *Phys. Chem. Chem. Phys.* **2021**, *23*, 5740−5749.
(44) Goettl, S. J.; Ahmed, M.; Mebel, A. M.; Kaiser, R. I. Molecular Mass Growth Processes to Polycyclic Aromatic Hydrocarbons through Radical−Radical Reactions Exploiting Photoionization Reflectron Time-of-Flight Mass Spectrometry. *Acc. Chem. Res.* **2025**, *58*, 2682−2694.
(45) Biswas, S.; Cokas, J.; Gee, W.; Paul, D.; Dias, N.; Morgan, H. W. T.; Finn, M. T.; Hudak, B. M.; Godbold, P. M.; Klug, C. A.; Epshteyn, A.; Alexandrova, A. N.; Ahmed, M.; Kaiser, R. I. Unconventional Low Temperature Decomposition of a Saturated Hydrocarbon over Atomically-Dispersed Titanium-Aluminum-Boron Catalyst. *Nat. Commun.* **2025**, *16*, No. 6793.
(46) Biswas, S.; Paul, D.; Dias, N.; Lu, W.; Ahmed, M.; Pantoya, M. L.; Kaiser, R. I. Efficient Oxidative Decomposition of Jet-Fuel exo-Tetrahydrodicyclopentadiene (JP-10) by Aluminum Nanoparticles in a Catalytic Microreactor: An Online Vacuum Ultraviolet Photoionization Study. *J. Phys. Chem. A* **2024**, *128*, 1665−1684.
(47) Jin, H.; Yang, J.; Xing, L.; Hao, J.; Zhang, Y.; Cao, C.; Pan, Y.; Farooq, A. An Experimental Study of Indene Pyrolysis with Synchrotron Vacuum Ultraviolet Photoionization Mass Spectrometry. *Phys. Chem. Chem. Phys.* **2019**, *21*, 5510−5520.
(48) Biswas, S.; Isakov, A.; Dias, N.; Finn, M. T.; Cokas, J.; Epshteyn, A.; Alexandrova, A. N.; Ahmed, M.; Kaiser, R. I. Low-Temperature Non-Oxidative Coupling of Methane on Atomically Dispersed Titanium−Aluminum−Boron Nanopowder. *J. Am. Chem. Soc.* **2026**, *148*, 10205−10215.
(49) Biswas, S.; Paul, D.; He, C.; Dias, N.; Ahmed, M.; Pantoya, M. L.; Kaiser, R. I. Counterintuitive Catalytic Reactivity of the Aluminum Oxide "Passivation" Shell of Aluminum Nanoparticles Facilitating the Thermal Decomposition of exo-Tetrahydrodicyclopentadiene (JP-10). *J. Phys. Chem. Lett.* **2023**, *14*, 9341−9350.
(50) Paul, D.; Biswas, S.; Dias, N.; Finn, M. T.; Lipton, A. S.; Epshteyn, A.; Ahmed, M.; Kaiser, R. I. A Synchrotron-Based Vacuum Ultraviolet Photoionization Mass Spectrometer-Coupled Microreactor To Probe Thermocatalysis. *Anal. Chem.* **2025**, *97*, 22846−22857.
(51) Biswas, S.; Goettl, S. J.; Krasnoukhov, V. S.; Dias, N.; Azyazov, V. N.; Arias, S.; Wnuk, S. F.; Ahmed, M.; Mebel, A. M.; Kaiser, R. I. Circumstellar Origin of Chrysene ($C_{18}H_{12}$) via Self-Recombination of Resonantly-Stabilized 1-Indenyl Radicals and Implications to the Aromaticity of the Carbonaceous Asteroid Ryugu. *Angew. Chem., Int. Ed.* **2026**, *65*, No. e8986387.
(52) Kaiser, R. I.; Zhao, L.; Lu, W.; Ahmed, M.; Krasnoukhov, V. S.; Azyazov, V. N.; Mebel, A. M. Unconventional Excited-State Dynamics in the Concerted Benzyl (C_7H_7) Radical Self-reaction to Anthracene ($C_{14}H_{10}$). *Nat. Commun.* **2022**, *13*, No. 786.
(53) Johansson, K. O.; Campbell, M. F.; Elvati, P.; Schrader, P. E.; Zádor, J.; Richards-Henderson, N. K.; Wilson, K. R.; Violi, A.; Michelsen, H. A. Photoionization Efficiencies of Five Polycyclic Aromatic Hydrocarbons. *J. Phys. Chem. A* **2017**, *121*, 4447−4454.
(54) Matsugi, A. Thermal Decomposition of Benzyl Radicals: Kinetics and Spectroscopy in a Shock Tube. *J. Phys. Chem. A* **2020**, *124*, 824−835.
(55) Buckingham, G. T.; Porterfield, J. P.; Kostko, O.; Troy, T. P.; Ahmed, M.; Robichaud, D. J.; Nimlos, M. R.; Daily, J. W.; Ellison, G. B. The Thermal Decomposition of the Benzyl Radical in a Heated Micro-Reactor. II. Pyrolysis of the Tropyl Radical. *J. Chem. Phys.* **2016**, *145*, No. 014305.
(56) Wentrup, C.; Winter, H.-W.; Kvaskoff, D. C_9H_8 Pyrolysis. o-Tolylacetylene, Indene, 1-Indenyl, and Biindenyls and the Mechanism of Indene Pyrolysis. *J. Phys. Chem. A* **2015**, *119*, 6370−6376.
(57) Semenikhin, A. S.; Savchenkova, A. S.; Chechet, I. V.; Matveev, S. G.; Liu, Z.; Frenklach, M.; Mebel, A. M. Rate Constants for H Abstraction from Benzo(a)pyrene and Chrysene: A Theoretical Study. *Phys. Chem. Chem. Phys.* **2017**, *19*, 25401−25413.
(58) Zhao, L.; Prendergast, M. B.; Kaiser, R. I.; Xu, B.; Ablikim, U.; Ahmed, M.; Sun, B.-J.; Chen, Y.-L.; Chang, A. H. H.; Mohamed, R. K.; Fischer, F. R. Synthesis of Polycyclic Aromatic Hydrocarbons by Phenyl Addition−Dehydrocyclization: The Third Way. *Angew. Chem., Int. Ed.* **2019**, *58*, 17442−17450.
(59) Kislov, V. V.; Mebel, A. M. The Formation of Naphthalene, Azulene, and Fulvalene from Cyclic C5 Species in Combustion: An Ab Initio/RRKM Study of 9-H-Fulvalenyl (C_5H_5−C_5H_4) Radical Rearrangements. *J. Phys. Chem. A* **2007**, *111*, 9532−9543.
(60) Zhao, L.; Kaiser, R. I.; Xu, B.; Ablikim, U.; Ahmed, M.; Joshi, D.; Veber, G.; Fischer, F. R.; Mebel, A. M. Pyrene Synthesis in Circumstellar Envelopes and its Role in the Formation of 2D Nanostructures. *Nat. Astron.* **2018**, *2*, 413−419.
(61) Sundar, S. P.; Al-Hammadi, S.; Ren, Z.; da Silva, G. Thermal Decomposition Kinetics of the Indenyl Radical: A Theoretical Study. *J. Phys. Chem. A* **2021**, *125*, 2782−2790.
(62) Matsugi, A.; Miyoshi, A. Reactions of o-Benzyne with Propargyl and Benzyl Radicals: Potential Sources of Polycyclic Aromatic Hydrocarbons in Combustion. *Phys. Chem. Chem. Phys.* **2012**, *14*, 9722−9728.
(63) He, C.; Thomas, A. M.; Galimova, G. R.; Morozov, A. N.; Mebel, A. M.; Kaiser, R. I. Gas-Phase Formation of Fulvenallene (C_7H_6) via the Jahn−Teller Distorted Tropyl (C_7H_7) Radical

Intermediate under Single-Collision Conditions. *J. Am. Chem. Soc.* **2020**, *142*, 3205−3213.
(64) Cau, P. Formation of Carbon Grains in the Atmosphere of IRC +10216. *Astron. Astrophys.* **2002**, *392*, 203−213.
(65) Kohn, D. W.; Clauberg, H.; Chen, P. Flash Pyrolysis Nozzle for Generation of Radicals in a Supersonic Jet Expansion. *Rev. Sci. Instrum.* **1992**, *63*, 4003−4005.
(66) Weddle, P. J.; Karakaya, C.; Zhu, H.; Sivaramakrishnan, R.; Prozument, K.; Kee, R. J. Boundary-Layer Model to Predict Chemically Reacting Flow within Heated, High-Speed, Microtubular Reactors. *Int. J. Chem. Kinet.* **2018**, *50*, 473−480.
(67) Frenklach, M.; Semenikhin, A. S.; Mebel, A. M. On the Mechanism of Soot Nucleation. III. The Fate and Facility of the E-Bridge. *J. Phys. Chem. A* **2021**, *125*, 6789−6795.
(68) Ziurys, L. M. The Chemistry in Circumstellar Envelopes of Evolved Stars: Following the Origin of the Elements to the Origin of Life. *Proc. Natl. Acad. Sci. U.S.A.* **2006**, *103*, 12274−12279.
(69) Lagadec, E.; Mékarnia, D.; de Freitas Pacheco, J. A.; Dougados, C. J. A. Dust Temperature and Density Profiles in the Envelopes of AGB and Post-AGB Carbon Stars from Mid-Infrared Observations. *Astron. Astrophys.* **2005**, *433*, 553−564.
(70) Sephton, M. A. Organic Compounds in Carbonaceous Meteorites. *Nat. Prod. Rep.* **2002**, *19*, 292−311.
(71) Mojarro, A.; Aponte, J. C.; Dworkin, J. P.; Elsila, J. E.; Glavin, D. P.; Connolly, H. C.; Lauretta, D. S. Prebiotic Organic Compounds in Samples of Asteroid Bennu Indicate Heterogeneous Aqueous Alteration. *Proc. Natl. Acad. Sci. U.S.A.* **2025**, *122*, No. e2512461122.
(72) Zeichner, S. S.; Aponte, J. C.; Bhattacharjee, S.; Dong, G.; Hofmann, A. E.; Dworkin, J. P.; Glavin, D. P.; Elsila, J. E.; Graham, H. V.; Naraoka, H.; et al. Polycyclic Aromatic Hydrocarbons in Samples of Ryugu Formed in the Interstellar Medium. *Science* **2023**, *382*, 1411−1416.
(73) Lecasble, M.; Remusat, L.; Viennet, J.-C.; Laurent, B.; Bernard, S. Polycyclic Aromatic Hydrocarbons in Carbonaceous Chondrites Can be Used as Tracers of Both Pre-Accretion and Secondary Processes. *Geochim. Cosmochim. Acta* **2022**, *335*, 243−255.
(74) Sabbah, H.; Quitté, G.; Demyk, K.; Joblin, C. First Direct Detection of Large Polycyclic Aromatic Hydrocarbons On Asteroid (162173) Ryugu Samples: An Interstellar Heritage. *Nat. Sci.* **2024**, *4*, No. e20240010.
(75) Yabuta, H.; Cody, G. D.; Engrand, C.; Kebukawa, Y.; De Gregorio, B.; Bonal, L.; Remusat, L.; Stroud, R.; Quirico, E.; Nittler, L.; et al. Macromolecular Organic Matter in Samples of the Asteroid (162173) Ryugu. *Science* **2023**, *379*, No. eabn9057.
(76) Lovas, F. J.; McMahon, R. J.; Grabow, J.-U.; Schnell, M.; Mack, J.; Scott, L. T.; Kuczkowski, R. L. Interstellar Chemistry: A Strategy for Detecting Polycyclic Aromatic Hydrocarbons in Space. *J. Am. Chem. Soc.* **2005**, *127*, 4345−4349.
(77) Tachibana, S.; Sawada, H.; Okazaki, R.; Takano, Y.; Sakamoto, K.; Miura, Y. N.; Okamoto, C.; Yano, H.; Yamanouchi, S.; Michel, P.; et al. Pebbles and Sand on Asteroid (162173) Ryugu: In Situ Observation and Particles returned to Earth. *Science* **2022**, *375*, 1011−1016.

https://doi.org/10.1021/jacs.6c13214
J. Am. Chem. Soc. 2026, 148, 45728−45737